Hindawi Publishing Corporation
Journal of Chemistry
Volume 2016, Article ID 8285717, 9 pages
http://dx.doi.org/10.1155/2016/8285717

Research Article

Synthesis of α-MnO_2 Nanomaterial from a Precursor γ-MnO_2: Characterization and Comparative Adsorption of Pb(II) and Fe(III)

Van-Phuc Dinh,[1] Ngoc-Chung Le,[2] Thi-Phuong-Tu Nguyen,[1] and Ngoc-Tuan Nguyen[3]

[1]*Dong Nai University, Tan Hiep Ward, Biên Hòa City, Đồng Nai Province, Vietnam*
[2]*Dalat University, Dalat City, Lâm Đồng Province, Vietnam*
[3]*Vietnam Atomic Energy Institute, Hanoi, Vietnam*

Correspondence should be addressed to Van-Phuc Dinh; dinhvanphuc82@gmail.com

Received 27 July 2016; Accepted 8 September 2016

Academic Editor: Frederic Dumur

α-MnO_2 nanostructure was successfully synthesized via hydrothermal treatment of a precursor γ-MnO_2. Structure, morphology, and BET surface area were characterized using X-ray powder diffraction (XRD), Scanning Electron Microscopy (SEM), and Brunauer-Emmett-Teller nitrogen adsorption (BET-N_2 adsorption). Thermal analysis result showed that α-MnO_2 nanorods were formed from γ-MnO_2 at 600°C. In addition, Pb(II) and Fe(III) adsorptive properties were investigated in an optimal condition. Results showed that equilibrium adsorption was obtained after 60 minutes for Pb(II) at pH = 4.0 and 80 minutes for Fe(III) at pH = 3.5 with 240 rpm of shaking speed overall. Experimental data was analyzed using three models: Langmuir, Freundlich, and Sips. Adsorption capacities (q_m) from the Langmuir isotherm models are 124.87 mg/g for Pb(II) and 30.83 mg/g for Fe(III). Along with the highest corelation coefficients, it is clear that the adsorption of Pb(II) and Fe(III) ions on α-MnO_2 surface followed Sips model. Kinetic studies indicated that the uptake of Pb(II) and Fe(III) occurred in the pseudo-second-order model with two stages for Pb(II) and three stages for Fe(III).

1. Introduction

Nowadays, the human health and the environment are in danger owing to the increase in industrial and mining activities [1]. Lead and iron ions seriously affect human life even in trace concentrations. According to the Environmental Quality Act, the limit for lead and iron in water is less than 0.1 mg/L and 1.0 mg/L. Therefore, there are many physicochemical treatments used to remove them, such as chemical precipitation, adsorption and ionic exchange, membrane technology, and solvent extraction. One of the most efficient and promising methods for treatment of lead and iron ions from an aqueous solution is the adsorption technology because of its high enrichment efficiency and ease of phase separation [2].

Being well known as a low-cost and environmentally friendly material, manganese oxides have been studied and applied to different areas since they have a great number of crystalline structures (α, β, γ, δ, etc.) and excellent chemical characteristics. Li batteries which are one of the important applications have been widely studied [3–9]. In addition, MnO_2 has been used for catalysts [10–13], supercapacitors [7, 14–17], and so forth. In recent years, MnO_2 has been studied as an adsorbent to remove inorganic as well as organic compounds from aqueous solution [8, 18–22]. However, adsorptive properties of α-MnO_2 nanomaterial as well as comparative adsorption of Pb(II) and Zn(II) onto this material are seldom reported.

In this study, α-MnO_2 was synthesized from heating precursor γ-MnO_2 and used as an adsorbent to remove Pb(II) and Zn(II) from an aqueous solution in an optimal condition. Comparative adsorption of two ions on α-MnO_2 was also investigated using three isotherm models: Langmuir, Freundlich, and Sips. The uptake kinetics were analyzed using

pseudo-first-order and pseudo-second-order models. In addition, intraparticle diffusion kinetics were also studied to ascertain the mechanism of the uptake.

2. Materials and Methods

2.1. Preparation of α-MnO_2 from γ-MnO_2. γ-MnO_2 which was successfully synthesized by Le and Van Phuc [2] from ethanol and potassium permanganate was heated at 600°C. The product after being investigated by XRD, SEM, and BET was used as an absorbent to remove lead and iron ions from the aqueous solution.

2.2. Adsorbent. Lead(II) and iron(II) ions were used as adsorbates. 1000 mg/L standard stock solution of each metal ion was prepared by dissolving $Pb(NO_3)_2$ and $Fe(NO_3)_3$ in distilled water.

2.3. Instruments. X-ray diffractometer D5000 made in Germany by Siemens with X-ray radiation CuKα, λ = 1,54056 Å, was used to examine the phase of the crystalline structure.

The morphology of the material was investigated by Ultra High Resolution Scanning Electron Microscopy S-4800, a transmission electron microscope.

Atomic Absorption Spectrophotometer (Atomic Absorption Spectrometer AA-7000 made in Japan by Shimadzu) was used to determine the BET surface area and pore site.

The pH measurements were done with a pH meter (Martini Instruments Mi-150, Romania); the pH meter was standardized using Hanna Instruments buffer solutions with pH values of 4.01 ± 0.01, 7.01 ± 0.01, and 10.01 ± 0.01.

A temperature-controlled shaker (Model IKA R5) was used for equilibrium studies.

2.4. Diagram for These Studies. See Figure 1.

2.5. Adsorption Study. 50 mL solution of heavy metal (Pb^{2+} and Zn^{2+}) ions was placed into a 100 mL conical flask containing 0.1 g α-MnO_2. During the uptake, influence of pH of the initial solution was adjusted within 2–5 range using HNO_3 0.1 M or NaOH 0.1 M solutions. Adsorption studies were also conducted in batch experiments with various adsorption times (20–240 minutes) and concentrations of metal ion (100–500 mg/L). Concentrations of heavy metal ions in the filtrate before and after uptake were determined using AAS.

Adsorption capacity was calculated by using the mass balance equation for the adsorption [1]:

$$q = \frac{(C_0 - C_e) \cdot V}{m}. \quad (1)$$

And the adsorption efficiency (%) was calculated from the formula

$$\%\ \text{Removal} = \frac{(C_0 - C_e) \cdot 100\%}{C_0}, \quad (2)$$

where q is the adsorption capacity (mg/g) at equilibrium, C_0 and C_e are the initial and the equilibrium concentrations (mg/L), respectively, V is the volume (L) of the solution, and m is the mass (g) of the adsorbent used.

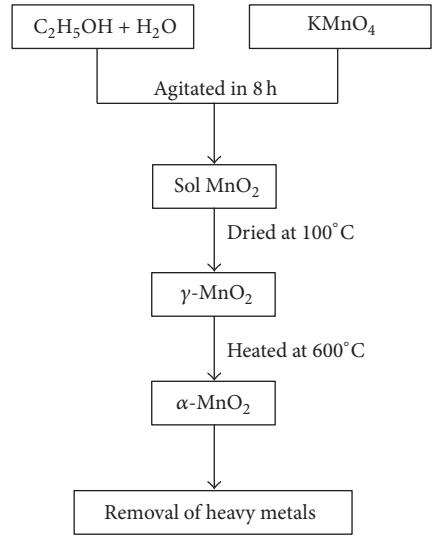

Figure 1

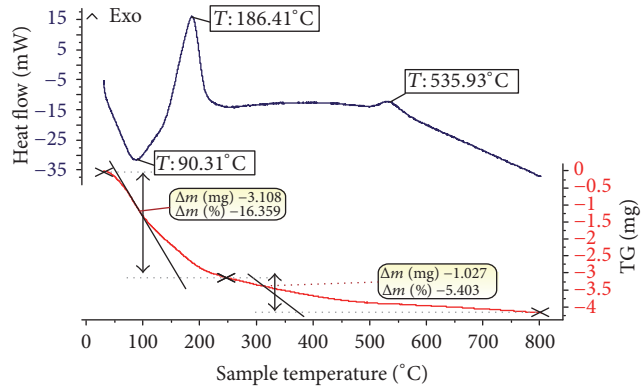

Figure 2: TG-DTA analysis.

3. Results and Discussion

3.1. Characterization of α-MnO_2 Nanostructures

3.1.1. Thermal Analysis Result. Thermal analysis (Figure 2) showed that there were two specific peaks corresponding to the decrease in volume of a product. From 100°C to 300°C, the endothermic process occurred which combined with a significant reduction of volume (approximately 16.40%) showed chemical dehydration as well as melting of material at 186.41°C. From 300°C to 800°C, there was a slight decrease in volume of about 5.40% which was the continued melting. In addition, there was an endothermic peak at 535.93°C corresponding to allotropic transformation. It was predicted that α-MnO_2 crystalline structure can be formed at above 536°C.

3.1.2. X-Ray Analysis Results. XRD analysis results showed that α-MnO_2 crystalline structure was not formed at 400°C (Figure 3). At higher temperatures, 600°C and 800°C, α-MnO_2 crystalline structure was completely formed with some specific peaks at 2θ = 28.58, 37.48, 49.78, 59.98, and 68.98 corresponding to the Miller indices (3 1 0), (2 1 1), (4 1 1), (5 2 1),

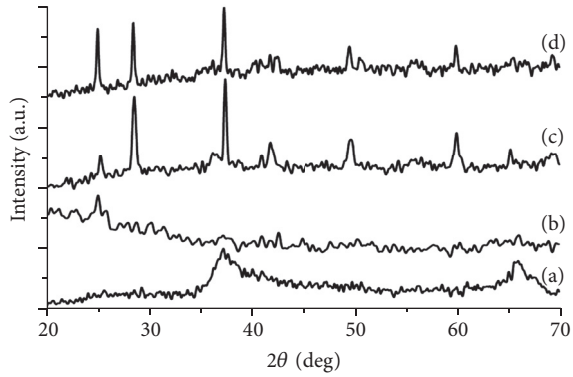

Figure 3: XRD image of MnO_2 at different temperatures: gamma-MnO_2 (a); t = 400°C (b); t = 600°C (c); and t = 800°C (d).

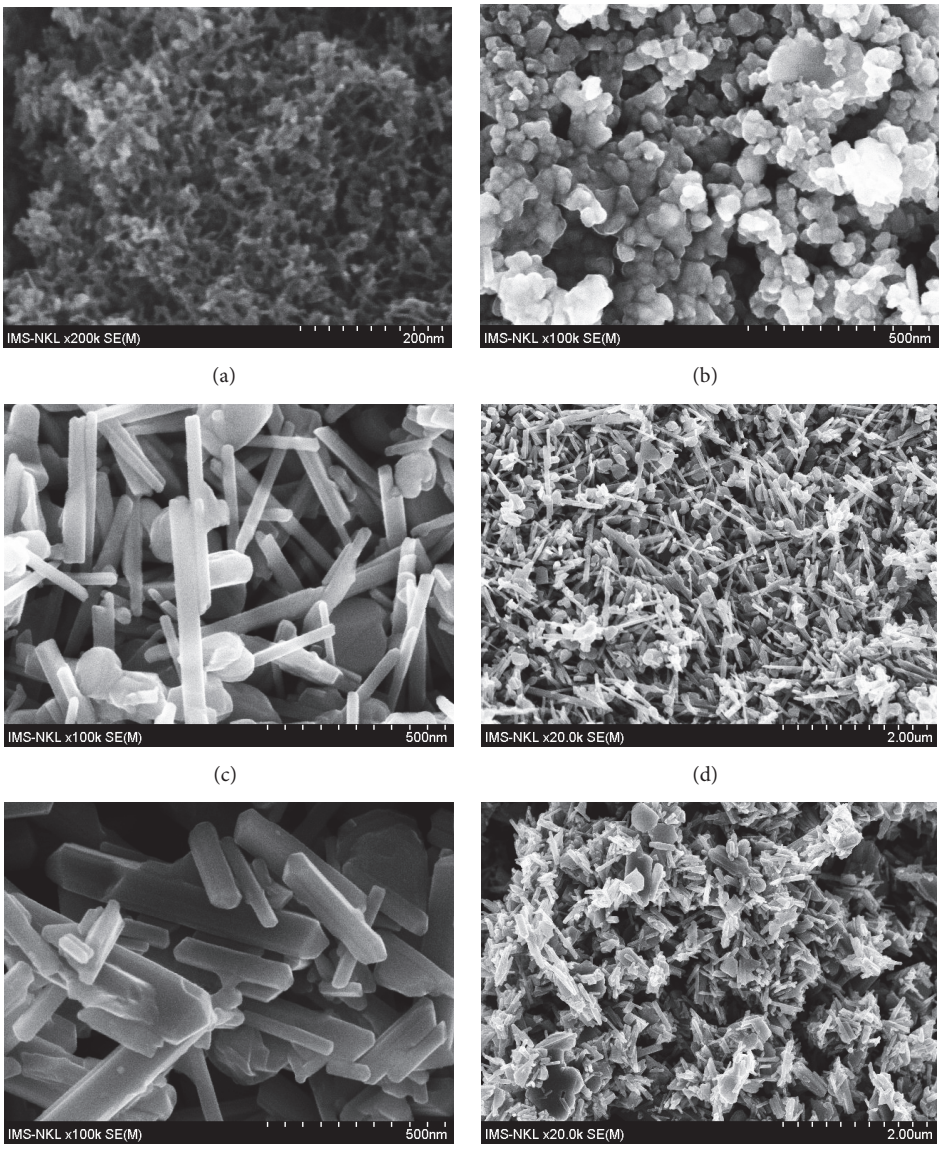

Figure 4: SEM images of material at 100°C (a), 400° (b), 600°C ((c), (d)), and 800°C ((e), (f)).

Table 1: BET and BJH analysis results of γ-MnO_2 and α-MnO_2.

Material	BET surface area	BJH adsorption pore size	BJH desorption pore size
γ-MnO_2	65.00 $m^2 \cdot g^{-1}$	417.83 Å	340.23 Å
α-MnO_2	9.37 $m^2 \cdot g^{-1}$	162.95 Å	734.37 Å

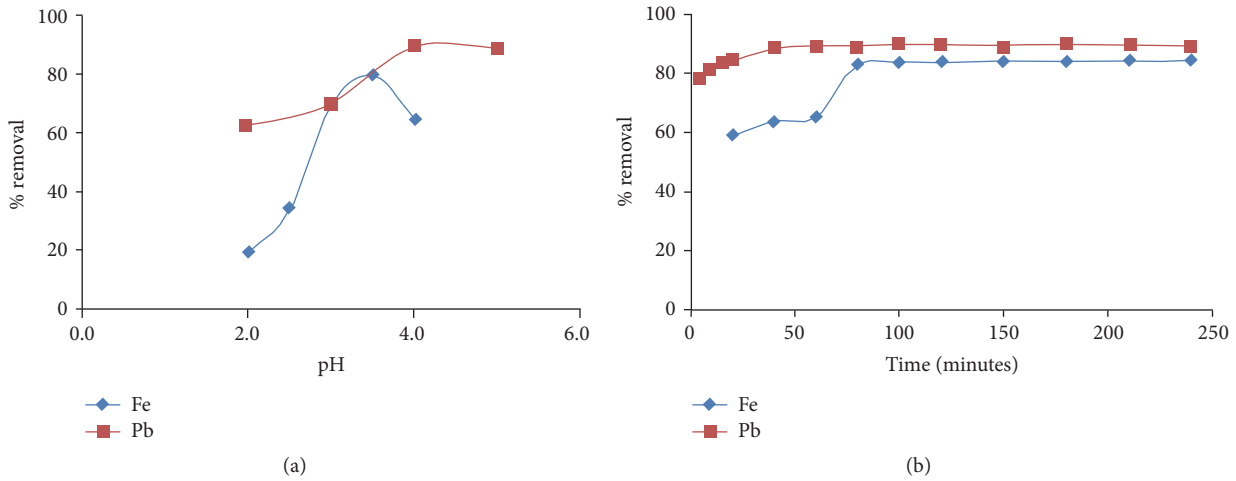

Figure 5: Influence of pH (a) and contact time (b) on adsorption of Pb(II) and Fe(III) at room temperature with 240 rpm of shaking speed.

and (5 4 1), respectively (ref. code: 01-072-1982). These results corresponded with prognostication from thermal analysis.

3.1.3. Scanning Electron Microscopy Analysis Results. Figure 4 showed that although γ-MnO_2 particles were flocculated at 400°C, the morphology of material was not changed. It can be concluded that α-MnO_2 nanostructures were not formed. At 600°C and 800°C, the morphology of the material was changed from nanospheres to nanorods which coincided with α-MnO_2 crystalline nanostructure corresponding to XRD results. However, these nanorods were broken and smashed at 800°C.

3.1.4. BET Surface Area and BJH Analysis. The BET surface area as well as BJH adsorption-desorption pore size of α-MnO_2 and γ-MnO_2 was provided in Table 1. Whereas precursor γ-MnO_2 had a BET surface area of about 65 $m^2 \cdot g^{-1}$, the synthesized α-MnO_2 had smaller surface, approximately 9.4 $m^2 \cdot g^{-1}$. This can be explained by the fact that γ-MnO_2 was composed of nanospheres, had a porous surface, and was small in size at room temperature. When heating γ-MnO_2 to form α-MnO_2 at 600°C, nanospheres were melted, flocculated, and showed an increase in size. As a result, α-MnO_2 had a smaller surface area than precursor γ-MnO_2. Both γ-MnO_2 and α-MnO_2 had BJH adsorption average pore width from 20 Å to 50 Å which were mesopores materials. However, with the fact that BJH adsorption pore size of γ-MnO_2 is smaller than that of α-MnO_2, it was revealed that adsorptive properties of γ-MnO_2 were better than those of α-MnO_2.

3.2. Adsorption Studies

3.2.1. Effective Factors. pH plays an important role in absorbing Pb(II) and Fe(III) ions onto α-MnO_2 material surface. At higher pH value, hydroxo ion MOH^{n+} or/and insoluble hydroxide $M(OH)_n$ was easily formed which inhibits the adsorption of these ions. In contrast, at low pH value, adsorption sites may be decreased because part of the MnO_2 nanomolecules can be dissolved in an acid solution as in the following reaction:

$$MnO_2 + 4H^+ + e^- \longrightarrow Mn^{2+} + 2H_2O \quad (3)$$

As a result, adsorption reached a maximum at pH = 4.0 for Pb(II) and pH = 3.5 for Fe(III) (Figure 5(a)).

Adsorption time is one of the important factors which helps us to predict kinetics as well as the mechanism of the uptake of heavy metals on material surface. The influence of contact time on the adsorption process of Pb(II) and Fe(III) onto α-MnO_2 was shown in Figure 5(b). As a result, the adsorption equilibrium was obtained after 60 minutes for Pb(II) and 80 minutes for Fe(III).

3.2.2. Isotherm Equation Studies. To understand the nature of the adsorption of Pb(II) and Fe(III) on material surface, some isotherm equations, such as Langmuir, Freundlich, and Sips, were investigated. While Langmuir model can help us to calculate the maximum adsorption capacity on a monolayer, Freundlich model shows the interaction between the absorbent and a multilayer. Plots of these nonlinear equations and equilibrium isotherm parameters were shown in Figure 6 and Table 2. Results showed that the maximum adsorption capacities calculated from Langmuir model were 124.87 mg/g for Pb(II) and 30.83 mg/g for Fe(III). This can be explained by the fact that lead ion is more satisfied with adsorption pore size because it has ion radius larger than iron. In addition,

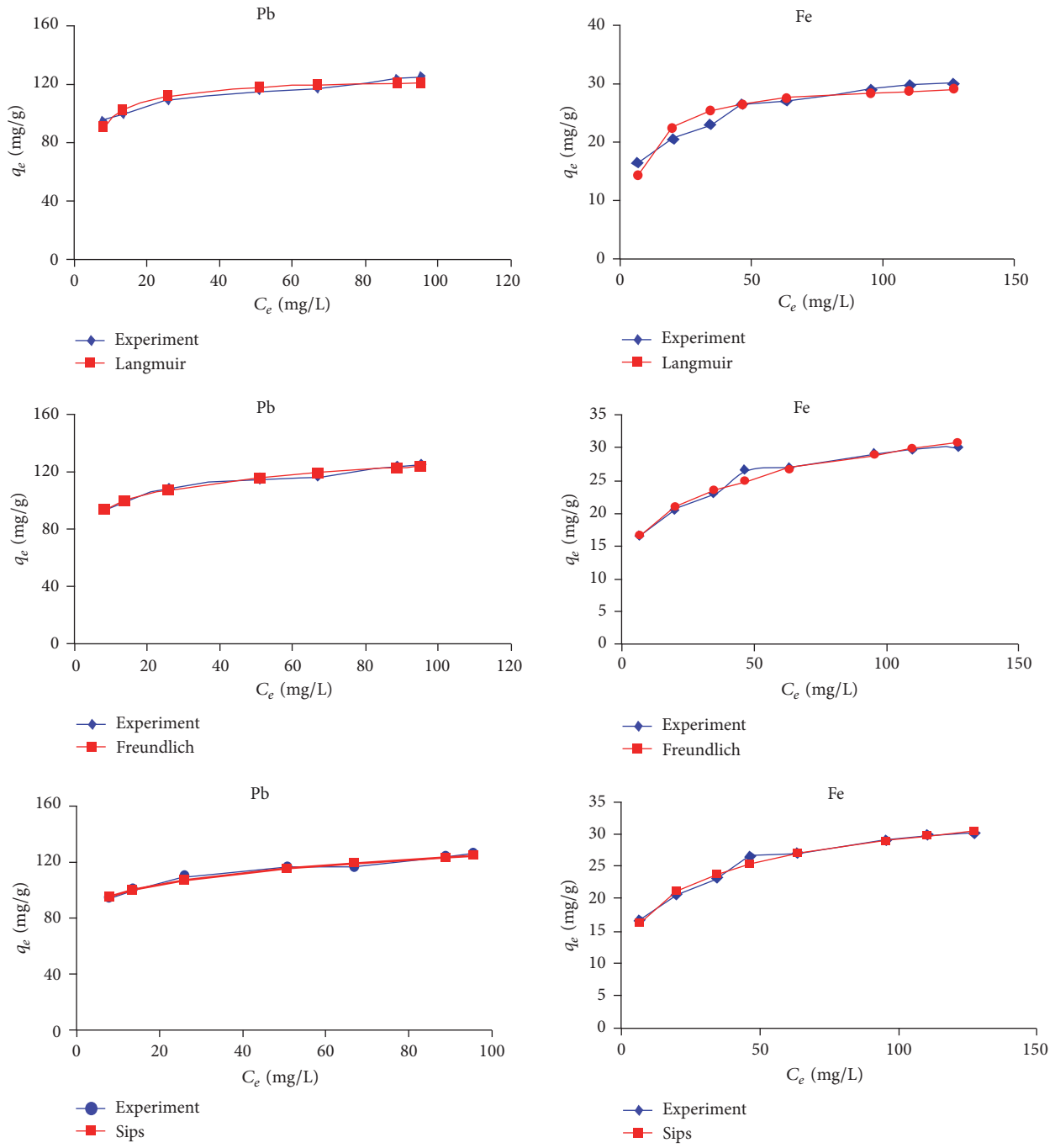

Figure 6: Plots of adsorption isotherm models: Langmuir, Freundlich, and Sips models.

the separation factor, S_F, which is a dimensionless constant equilibrium parameter, was given by

$$S_F = \frac{1}{1 + K_L \cdot C_0}. \quad (4)$$

Based on the S_F value, it can be revealed that the smaller the value of S_F is, the more favorable the adsorption is. The calculated S_F values which were smaller than 1 and higher than 0 in both the lowest and the highest concentrations showed that α-MnO_2 was an appropriate adsorbent for Fe(III) and Pb(II). However, S_F value of Pb(II) > Fe(III) indicated that Fe(III) will compete for binding sites faster than Pb(II) in a mixed metal ions system.

Moreover, the $1/n$ values calculated from Freundlich model for Fe(III) higher than Pb(II) indicated that the interaction between α-MnO_2 and Fe(III) is more favorable than α-MnO_2 and Pb(II).

However, the material surface shows heterogeneity. Hence, the uptake of heavy metal ions onto MnO_2 can occur on different mechanisms. Sips model, which is Langmuir and

Table 2: Equilibrium isotherm parameters.

Isotherm	Nonlinear forms	Isotherm parameters	Pb(II)	Fe(III)
Langmuir	$q_e = \frac{q_m \cdot K_L \cdot C_e}{1 + K_L \cdot C_e}$	K_L	0.3340	0.135
		q_m (mg/g)	124.9	30.83
		RMSE	3.529	1.504
		R^2	0.9109	0.9042
		χ^2	0.6618	0.7603
		S_F (at the lowest C_0)	0.0291	0.0689
		S_F (at the highest C_0)	$5.95{\cdot}10^{-3}$	0.0146
Freundlich	$q_e = K_F \cdot C_e^{1/n}$	$1/n$	0.1115	0.2033
		K_F	74.76	11.52
		RMSE	1.493	0.695
		R^2	0.9840	0.9795
		χ^2	0.1148	0.1296
Sips	$q_e = \frac{K_S \cdot C_e^{\beta_S}}{1 + \alpha_S \cdot C_e^{\beta_S}}$	K_S	6.75	11.84
		α_S	−0.9142	0.1986
		β_S	0.0070	0.3442
		RMSE	1.4689	0.6272
		R^2	0.9846	0.9833
		χ^2	0.1133	0.1122

q_e: adsorption capacity at equilibrium (mg/g); q_m: maximum adsorption capacity (mg/g); C_e: equilibrium concentration (mg/L); K_L: Langmuir constant; K_F: Freundlich constant; n: adsorption intensity; K_S: Sips constant; α_S: Sips isotherm model constant (L/mg); β_S: Sips isotherm model exponent; R^2: correlation coefficient; RMSE: root mean square error; χ^2: nonlinear chi-square test.

Freundlich models combined, generally described exactly the nature of adsorption. Sips isotherm equation was given by formula [1]

$$q_e = \frac{K_S \cdot C_e^{\beta_S}}{1 + \alpha_S \cdot C_e^{\beta_S}}, \quad (5)$$

where α_S is Sips isotherm model constant (L/mg); β_S is Sips isotherm model exponent; K_S is Sips constant; C_e (mg/L) is the equilibrium concentration; and q_e (mg/g) is adsorption capacity. Sips equation is a three-parameter model, and thus it can be solved by Solver Add-In in Microsoft Excel.

In comparison with the correlation coefficients (R^2), the root mean square error (RMSE), and the nonlinear chi-square test (χ^2) values of the three models, it was clear that the adsorption of Pb(II) and Fe(III) onto α-MnO_2 followed Sips model due to the highest R^2 value as well as the lowest RMSE and χ^2 ones.

3.2.3. Kinetic Studies. Pseudo-first-order and pseudo-second-order models are often used to describe the uptake of heavy metal ions onto material surface for adsorption time. Kinetic parameters give essential information for designing and modeling the adsorption processes. However, the two modes cannot determine clearly the nature of the adsorption of Pb(II) and Fe(III) onto α-MnO_2 nanomaterial. Therefore, intraparticle diffusion model which was developed by Weber and Morris was applied for ascertaining a mechanism of the uptake of Pb(II) and Fe(III) onto α-MnO_2. Plots of these kinetic models were shown in Figure 7 and kinetic parameters were given in Table 3.

Results showed that the theoretical q_e values which were calculated from pseudo-second-order kinetic models were more accordant with the experimental values, $q_{e(\exp)}$, than pseudo-first-order kinetic ones. In addition, correlation coefficients in these pseudo-second-order kinetic models for both Pb(II) and Fe(III) were higher than 0.9950. It was revealed that pseudo-second-order models were satisfied with describing kinetics of the uptake of Pb(II) and Fe(III) on α-MnO_2.

Furthermore, intraparticle diffusion models showed that the uptake of Pb(II) followed two stages: firstly, Pb(II) ions were quickly adsorbed on α-MnO_2 surface; secondly, there was gradual diffusion of absorbents from surface sites into the inner pores. And it was observed that there are three stages in the sorption of Fe(III) ion on the material surface. In the first one, Fe(III) ion was rapidly transferred from the solution to α-MnO_2 surface. In the next one, intraparticle diffusion which is the controlling factor gradually occurred. Lastly, the adsorption equilibrium was obtained to correspond with the saturation of absorbent sites. The intraparticle diffusion constants for all these stages were given in Table 3.

4. Conclusion

In this report, α-MnO_2 nanostructure synthesized from a precursor γ-MnO_2 was used as an adsorbent to remove Pb(II) and Fe(III) from an aqueous solution at an optimal

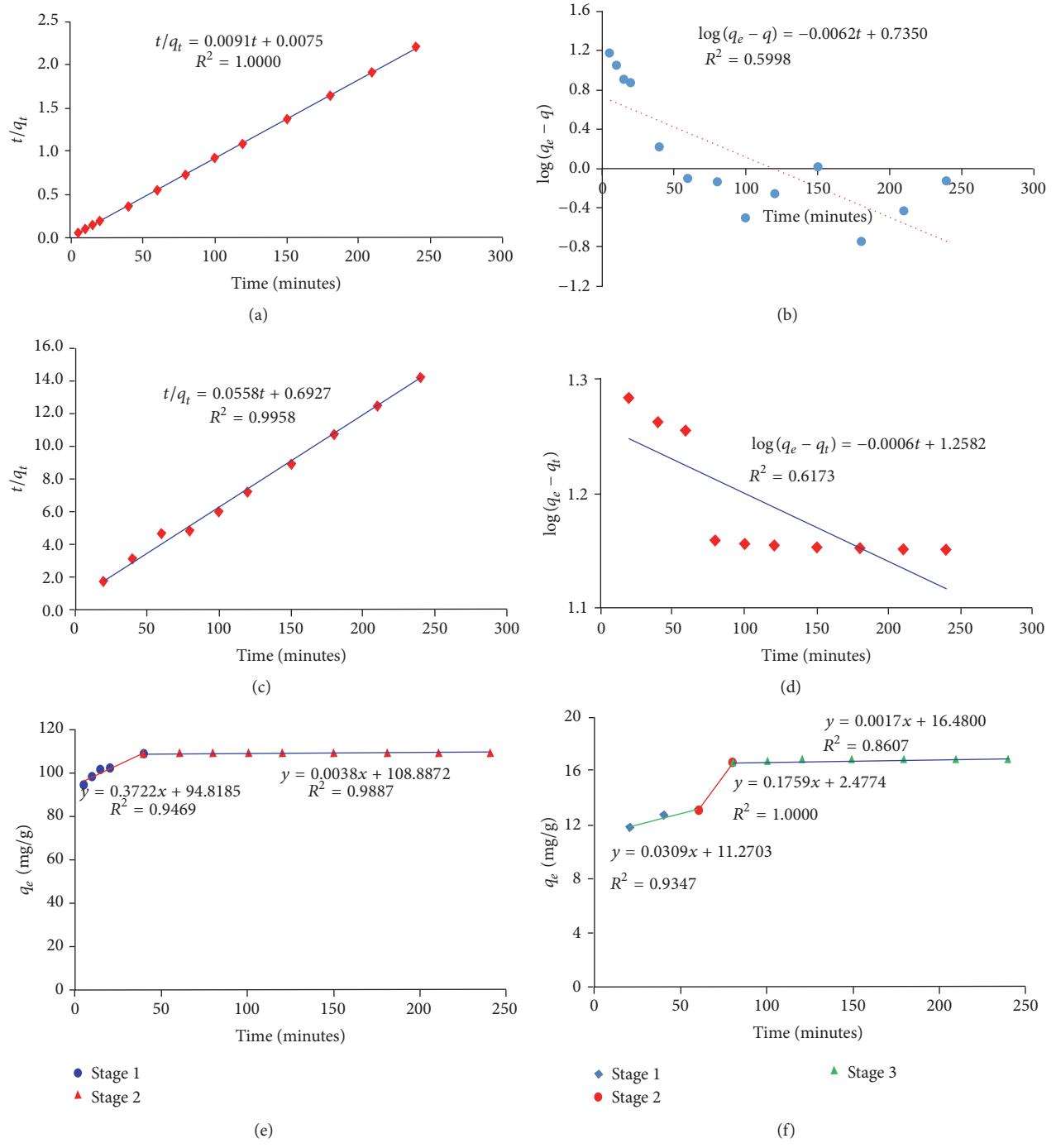

FIGURE 7: Pseudo-first-order kinetic plots for the adsorption of Pb(II) (a) and Fe(III) (c). Pseudo-second-order kinetic plots for the adsorption of Pb(II) (b) and Fe(III) (d). Intraparticle diffusion kinetic plots for the adsorption of Pb(II) (e) and Fe(III) (f).

condition. Results showed that the maximum capacities were 124.87 mg/g for Pb(II) and 30.83 mg/g for Fe(III) at pH = 4.0 for Pb(II) and pH = 3.5 for Fe(III). Experiment data which was analyzed using three isotherm models, that is, Langmuir, Freundlich, and Sips, indicated that Sips model was fitted better than the other two. Kinetics studies showed that both Pb(II) and Fe(III) corresponded with pseudo-second-order model with corelation coefficient constants (R^2) higher than 0.9950. Intraparticle diffusion kinetics confirmed that the uptake of Pb(II) on α-MnO_2 includes two stages while it includes three stages for Fe(III).

Competing Interests

The authors declare that there are no competing interests regarding the publication of this paper.

Table 3: Kinetic parameters.

Kinetic models	Linear forms	Kinetic parameters		
			Pb(II)	Fe(III)
		$q_{e(\exp)}$ (mg/g)	109.80	16.80
Pseudo-first-order model $\frac{dq}{dt} = K_1 (q_e - q)$	$\log (q_e - q_t) = \log q_e - \frac{K_1 \cdot t}{2{,}303}$	K_1 ($\min^{-1}$)	0.01428	$1.38{\cdot}10^{-3}$
		R^2	0.5998	0.6873
		$q_{e(\text{cal})}$ (mg/g)	5.433	18.12
Pseudo-second-order model $\frac{dq}{dt} = K_2 (q_e - q)^2$	$\frac{t}{q} = \frac{1}{K_2 q_e^2} + \left(\frac{1}{q_e}\right) \cdot t$	K_2 ($\text{g}{\cdot}\text{mg}^{-1}{\cdot}\min^{-1}$)	0.01108	$4.5{\cdot}10^{-3}$
		R^2	1.000	0.9958
		$q_{e(\text{cal})}$ (mg/g)	109.89	17.92
Intraparticle diffusion model	$q_t = K_d t^{1/2} + C$	K_{d1}	0.3722	0.0309
		K_{d2}	0.0038	0.1759
		K_{d3}		0.0017

References

[1] K. Y. Foo and B. H. Hameed, "Insights into the modeling of adsorption isotherm systems," *Chemical Engineering Journal*, vol. 156, no. 1, pp. 2–10, 2010.

[2] N. C. Le and D. Van Phuc, "Sorption of lead (II), cobalt (II) and copper (II) ions from aqueous solutions by γ-MnO_2 nanostructure," *Advances in Natural Sciences: Nanoscience and Nanotechnology*, vol. 6, no. 2, Article ID 025014, 2015.

[3] M. M. Thackeray and A. De Kock, "Synthesis of γ-MnO_2 from $LiMn_2O_4$ for Li/MnO_2 battery applications," *Journal of Solid State Chemistry*, vol. 74, no. 2, pp. 414–418, 1988.

[4] S. Sarciaux, A. Le Gal La Salle, A. Verbaere, Y. Piffard, and D. Guyomard, "γ-MnO_2 for Li batteries Part I. γ-MnO_2: relationships between synthesis conditions, material characteristics and performances in lithium batteries," *Journal of Power Sources*, vol. 81-82, pp. 656–660, 1999.

[5] K. S. Abou-El-Sherbini, "Structure investigation and electrochemical behavior of γ-MnO_2 synthesized from three-dimensional framework and layered structures," *Journal of Solid State Chemistry*, vol. 166, no. 2, pp. 375–381, 2002.

[6] L. I. Hill, A. Verbaere, and D. Guyomard, "MnO_2 (α-, β-, γ-) compounds prepared by hydrothermal-electrochemical synthesis: characterization, morphology, and lithium insertion behavior," *Journal of Power Sources*, vol. 119–121, pp. 226–231, 2003.

[7] Y. Li, H. Xie, J. Wang, and L. Chen, "Preparation and electrochemical performances of α-MnO_2 nanorod for supercapacitor," *Materials Letters*, vol. 65, no. 2, pp. 403–405, 2011.

[8] J. Li, B. Xi, Y. Zhu, Q. Li, Y. Yan, and Y. Qian, "A precursor route to synthesize mesoporous γ-MnO_2 microcrystals and their applications in lithium battery and water treatment," *Journal of Alloys and Compounds*, vol. 509, no. 39, pp. 9542–9548, 2011.

[9] M. R. Bailey and S. W. Donne, "Structural effects on the cyclability of the alkaline γ-MnO_2 electrode," *Electrochimica Acta*, vol. 56, no. 14, pp. 5037–5045, 2011.

[10] L. Jin, C.-H. Chen, V. M. B. Crisostomo, L. Xu, Y.-C. Son, and S. L. Suib, "γ-MnO_2 octahedral molecular sieve: preparation, characterization, and catalytic activity in the atmospheric oxidation of toluene," *Applied Catalysis A: General*, vol. 355, no. 1-2, pp. 169–175, 2009.

[11] T. Lin, L. Yu, M. Sun, G. Cheng, B. Lan, and Z. Fu, "Mesoporous α-MnO_2 microspheres with high specific surface area: controlled synthesis and catalytic activities," *Chemical Engineering Journal*, vol. 286, pp. 114–121, 2016.

[12] Y. Wu, S. Li, Y. Cao, S. Xing, Z. Ma, and Y. Gao, "Facile synthesis of mesoporous α-MnO_2 nanorod with three-dimensional frameworks and its enhanced catalytic activity for VOCs removal," *Materials Letters*, vol. 97, pp. 1–3, 2013.

[13] X. Fu, J. Feng, H. Wang, and K. M. Ng, "Manganese oxide hollow structures with different phases: synthesis, characterization and catalytic application," *Catalysis Communications*, vol. 10, no. 14, pp. 1844–1848, 2009.

[14] H. Wei, J. Wang, S. Yang, Y. Zhang, T. Li, and S. Zhao, "Facile hydrothermal synthesis of one-dimensional nanostructured α-MnO_2 for supercapacitors," *Physica E: Low-dimensional Systems and Nanostructures*, vol. 83, pp. 41–46, 2016.

[15] N. Boukmouche, N. Azzouz, L. Bouchama, A. Lise Daltin, J. Paul Chopart, and Y. Bouznit, "Supercapacitance of MnO_2 films prepared by pneumatic spray method," *Materials Science in Semiconductor Processing*, vol. 27, no. 1, pp. 233–239, 2014.

[16] M. Pang, G. Long, S. Jiang et al., "One pot low-temperature growth of hierarchical δ-MnO_2 nanosheets on nickel foam for supercapacitor applications," *Electrochimica Acta*, vol. 161, pp. 297–304, 2015.

[17] Z. Li, Z. Liu, B. Li et al., "Large area synthesis of well-dispersed β-MnO_2 nanorods and their electrochemical supercapacitive performances," *Journal of the Taiwan Institute of Chemical Engineers*, vol. 65, pp. 544–551, 2016.

[18] D. Nguyen Thanh, M. Singh, P. Ulbrich, N. Strnadova, and F. Štěpánek, "Perlite incorporating γ-Fe_2O_3 and α-MnO_2 nanomaterials: preparation and evaluation of a new adsorbent for As(V) removal," *Separation and Purification Technology*, vol. 82, no. 1, pp. 93–101, 2011.

[19] M. Wang, P. Pang, L. K. Koopal, G. Qiu, Y. Wang, and F. Liu, "One-step synthesis of δ-MnO_2 nanoparticles using ascorbic acid and their scavenging properties to Pb(II), Zn(II) and methylene blue," *Materials Chemistry and Physics*, vol. 148, no. 3, pp. 1149–1156, 2014.

[20] Y. Du, G. Zheng, J. Wang, L. Wang, J. Wu, and H. Dai, "MnO_2 nanowires in situ grown on diatomite: highly efficient absorbents for the removal of Cr(VI) and As(V)," *Microporous and Mesoporous Materials*, vol. 200, pp. 27–34, 2014.

[21] X. Ge, J. Liu, X. Song et al., "Hierarchical iron containing γ-MnO_2 hollow microspheres: a facile one-step synthesis and

effective removal of As(III) via oxidation and adsorption," *Chemical Engineering Journal*, vol. 301, pp. 139–148, 2016.

[22] M. Gheju, I. Balcu, and G. Mosoarca, "Removal of Cr(VI) from aqueous solutions by adsorption on MnO_2," *Journal of Hazardous Materials*, vol. 310, pp. 270–277, 2016.